npj | heritage science

Article

https://doi.org/10.1038/s40494-025-02289-3

Heritage knowledge meets microclimate: CFD–UTCI validation of Eight Mansions orientation in southern Fujian, China

Check for updates

Yaolong Wang[1], Jiarui Xu[2], Yingning Shen[3], Lei Wang[1], Fengliang Tang[1], Tiantian Huang[1], Tingfeng Liu[1] ✉ & Zefa Wang[1] ✉

We test whether orientation rules in the Eight Mansions (Ba Zhai) tradition align with microclimatic comfort in a hot–humid setting. Using CFD coupled with the Universal Thermal Climate Index (UTCI), we simulated 24 rotational orientations of a typical ancestral hall in Quanzhou, China, under summer boundary conditions. Orientations aligning the courtyard opening with prevailing south-easterly winds produced lower median UTCI, with inter-orientation differences of ~0.3 °C. Across orientations, mean radiant temperature varied little, whereas airflow differences dominated comfort outcomes. 'Auspicious' categories overlapped with the best-performing orientations, and Feng Shui scores correlated with UTCI ($\rho = -0.60$, $p = 0.002$) in this case study. The results frame traditional orientation heuristics as testable hypotheses and suggest context-specific pathways for climate-adaptive conservation and design.

Global warming has become a severe challenge facing contemporary human society. According to the Intergovernmental Panel on Climate Change, the global mean surface temperature has risen by about 1.1 °C relative to the pre-industrial level over recent decades, and the warming trend continues to intensify[1]. Meanwhile, energy-related carbon emissions from the building sector account for roughly 27% of global emissions[2]. The energy demand driven by air-conditioning has risen markedly, further reinforcing the vicious cycle between climate change and building energy consumption. Evidence indicates that each 1 °C increase in urban temperature leads to an approximately 2–4% rise in peak air-conditioning energy demand[3]. Consequently, exploring passive strategies for thermal-environment regulation that both adapt to climate change and reduce building energy use has become a key research topic in architecture and urban–rural planning[4].

In contrast to the widespread reliance of modern buildings on active mechanical cooling, traditional Chinese architecture has, through long-term climatic adaptation, developed a rich repertoire of passive environmental regulation strategies—such as rational spatial layout, optimised orientation, shading design, and ventilation organisation—to achieve harmony between buildings and their surroundings[5,6]. These forms of traditional ecological wisdom have been shown in practice to improve the building microclimate, reduce sensible-heat accumulation, and lower air-conditioning energy consumption, aligning with the goals of low-carbon buildings and sustainable urban development [7,8].

Traditional Feng Shui theory has been embedded in the practice of creating human settlements in China for more than two millennia. Its core concerns the coordination of "form–principle–human": external landform (xingfa), directional qi field (lifa) and the household (ren) are matched to pursue auspiciousness and avoid inauspiciousness (see Fig. 1 for schematic landscape configuration). From the 1980s–1990s, scholarship first focused on its ecological-adaptation core. Wang (2005) further viewed Feng Shui as a concentrated expression of the Chinese architectural "environmental view", stressing that the triadic coupling of "form–principle–human" accords closely with contemporary sustainable-design principles[9]. Cheng (2010) positioned Feng Shui as "ancient environmental engineering", noting that the emphasis on terrain safety and water security in site selection is consistent with modern ecological design, while distinguishing between quantifiable xingfa and taboo-coloured lifa[10]. Through comparative studies of settlements "backing mountains and facing water," Liang (1988) argued that Feng Shui patterns balance defensibility and resource accessibility[11]. Subsequently, Liu (1996) proposed the "Hutian" pattern—where a basin interior is connected to an external corridor via a gap—as pervasive on the Loess Plateau, indicating that Feng Shui is not superstition but an experiential summary of regional micro-topography and micro-climate adaptation [12].

In the twenty-first century, research has shifted towards systematisation and cross-disciplinary interpretation. Recent studies show that preference for orientation, planning of ventilation paths and courtyard

[1]School of Architecture, Tianjin University, Tianjin, China. [2]School of Humanities and Arts, Hainan College of Economics and Business, Haikou, China. [3]School of Cultural Heritage, Northwest University, Xi'an, Shaanxi, China. ✉e-mail: tfliu1967@tju.edu.cn; zefawang@qztc.edu.cn

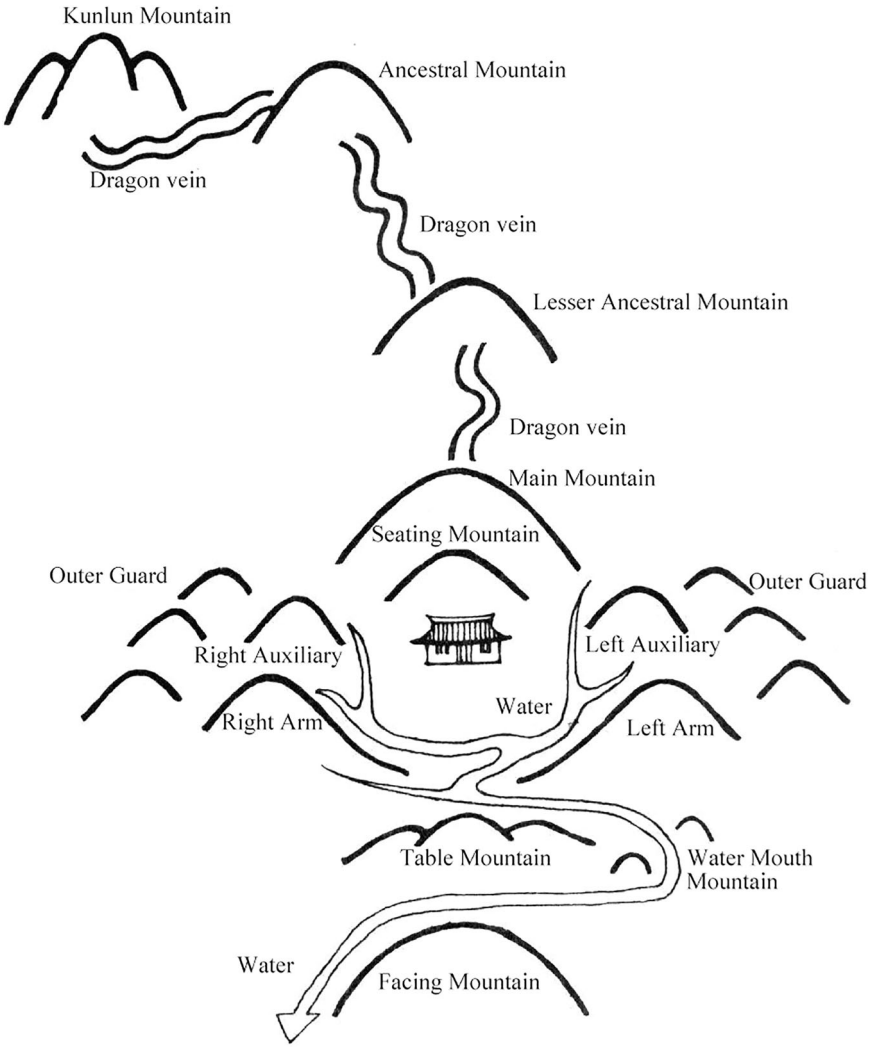

Fig. 1 | Traditional Feng Shui landscape configuration (schematic). The diagram summarizes key landform elements—main mountain, ancestral mountain, dragon veins, left/right arms and outer guards, water mouth and facing mountain—arranged around a settlement core. Elements are not to scale; English terms are used and Chinese names are provided at first mention in the text.

layout embodied in Feng Shui have a degree of scientific basis and practical value for improving indoor–outdoor microclimates and enhancing thermal comfort[13,14]. In China and East Asia, Feng Shui continues to shape the siting of vernacular settlements, courtyard patterns and woodland conservation, presenting an integrated environmental worldview of "landform–qi–culture"[15]. Regional investigations by Luo (2010) and Cheng (2002) illustrate how Hakka shuikou forests and ring-shaped tulou intended to "accumulate qi" serve both clan ethics and ecological suitability[16,17]. At the same time, international scholarship has begun to evaluate systematically the scientific validity and social benefits of Feng Shui. A systematic review of 36 Chinese and English empirical papers by Han and Lin (2023) reports positive correlations between Feng Shui environments and housing prices, forest ecological quality and wind-environment comfort, while noting that causal mechanisms for human health remain unverified; hence Feng Shui is "neither pure superstition nor strict science"[18]. From a philosophy-of-science perspective, Matthews (2019) critiques the difficulty of falsifying the concept of qi, urging methodological reflexivity between cultural interpretation and physical verification[19]. Together, these findings construct a dual cultural–ecological picture of Feng Shui studies and reveal ongoing debates over its scientific status.

Research outcomes have also extended to mental health and urban design. The "urban Feng Shui" model proposed by Shokri, Shieh and Vahid (2023) suggests that integrating Feng Shui principles into public-space design can enhance residents' well-being and environmental satisfaction[20]. In heritage contexts, Zhang's (2018) fieldwork demonstrates that Feng Shui, as "living heritage", participates in the construction of place identity and historical narrative[21]. Meanwhile, Bo and Su (2014) argue that the Feng Shui ideal of human–nature harmony aligns with green-building goals, offering a localised pathway for low-carbon design [22].

With advances in digital technology, CFD, GIS and in-situ monitoring have increasingly become mainstream means to test Feng Shui experience. Multi-scale simulations for Jiangmen, Guangdong by Li et al. show that layouts conforming to prevailing winds and courtyard enclosures can improve natural-ventilation efficiency by 15–25%[14]. Through summer measurements coupled with CFD, Guo et al. verified that courtyards in Beijing's Prince Kung's Mansion, consistent with Feng Shui principles increased the coverage of comfortable wind speeds by about 30% compared with control layouts[23]. Under winter conditions, Zhao, Zhang and Peng (2023) found that flanking "dragon" and "tiger" hills (longhu sha) help weaken cold-wind infiltration and improve indoor thermal comfort[24]. At the village scale, Zhou et al. (2022) demonstrated a significant spatial coupling between "backing mountains and facing water" siting and optimisation of the wind–thermal environment in Jinxi, Jiangxi[25]. At the micro scale, simulations reveal the physical mechanisms of traditional details—Wang et al. showed that, in siheyuan (courtyard houses), positioning the windward gate improves courtyard ventilation more effectively than orientation alone, corroborating the importance of the "door" among the "three essentials of a dwelling" (yangzhai san yao) [26].

In recent years, empirical studies on building climate adaptation have increasingly employed CFD, in-situ monitoring and GIS-based assessment,

providing preliminary evidence for the physical bases by which courtyard enclosures, shelterbelts and "back-to-mountain, facing-water" layouts improve microclimates[27–29]. However, most of this work relies on single or a few fixed orientations and focuses on partial operating conditions, such as summer ventilation or winter heat retention[30,31], lacking a systematic test of the universal proposition in traditional theory that "auspiciousness is determined by orientation". In particular, the Eight Mansions (Ba Zhai) school judges auspiciousness solely on the basis of building orientation, yet very few studies convert the full 360° spectrum of orientations into quantifiable thermal-environment indicators to verify whether the auspiciousness sequence is statistically associated with human heat stress.

The Minnan region is hot-humid with pronounced land–sea breeze diurnal cycles. Existing studies largely remain at the level of modelling or short-term field tests, without targeted evaluation of dynamic thermal comfort during extreme-heat weeks, and they also lack a unified rule set for quantifying auspiciousness to support cross-case comparison[32]. These gaps indicate the need, at the scale of a typical Minnan ancestral hall, to construct a comprehensive evaluation system covering multiple orientations and multiple indicators, and to test under the hottest conditions the statistical relationships between Eight Mansions auspicious orientations and thermal-comfort metrics such as UTCI, in order to clarify the scientific value embedded therein.

This study aims to use modern numerical simulation and human thermal-comfort evaluation methods to quantitatively analyse how orientation in typical Minnan courtyard houses in Quanzhou affects courtyard thermal environments and microclimates; it also seeks to systematically quantify and verify the association between the auspicious orientations recommended by the Eight Mansions Feng Shui theory and thermal-comfort levels, thereby revealing the climate adaptability and scientific connotations of traditional architectural experience.

As an important component of China's intangible cultural heritage, Eight Mansions Feng Shui embodies not only experience concerning building orientation and microclimate regulation but also a knowledge system accumulated over time, interweaving human–land relationships, cosmological concepts and place-based environmental wisdom. Accordingly, this study treats Feng Shui as a "heritage knowledge system" and uses numerical simulation and statistical methods to scientifically verify and re-contextualise its connotations. Such an approach helps to discern the potential scientific validity and limitations within traditional experience and provides new pathways for the contemporary translation and interdisciplinary safeguarding of intangible cultural heritage.

Methods

Assignment of auspiciousness values

This study adopts the Eight Mansions (Ba Zhai) school of Feng Shui for empirical verification. Originating in the Ming dynasty classic Ba Zhai Mingjing, this system uses a dwelling's sitting–facing direction (坐向) to assign a trigram (宅卦) and determine directional auspiciousness through a set of fixed correspondences with eight stars: Shengqi (生气), Tianyi (天医), Yannian (延年), Fuwei (伏位), Liusha (六煞), Wugui (五鬼), Huohai (祸害), and Jueming (绝命). The system is rule-based, quantifiable, and widely practiced in Minnan folk architecture [33,34].

Each of the 24 compass orientations (二十四山), spaced at 15° intervals (e.g., Zi at 0°, Gui at 15°, Chou at 30°), corresponds to a specific mountain (山) and direction (向). The sitting mountain determines the dwelling's trigram, and the Eight Mansions rules then map the eight stars around the compass in a fixed pattern unique to each trigram. For instance, a 坎宅 (Kan trigram house) distributes the eight stars clockwise starting from Fuwei at Kan itself (0°).

To convert this symbolic system into a usable numerical variable for statistical testing, we adopted a nine-level ordinal scale based on Yangzhai Shishu and Feng Shui manuals: Shengqi (生气) = +4, Tianyi (天医) = +3, Yannian (延年) = +2, Fuwei (伏位) = +1, Centre = 0, Huohai (祸害) = −1, Liusha (六煞) = −2, Wugui (五鬼) = −3, and Jueming (绝命) = −4.

This mapping preserved the ordinal nature of auspiciousness while enabling correlation with continuous variables. Table 1 and Fig. 2 show the full assignment across 24 orientations. The resulting scoring framework allows orientation-based simulation results to be directly compared with traditional Feng Shui expectations.

To account for the building's rotation, the sitting–facing direction (坐山–朝向) was updated in 15° increments. For each new orientation, the trigram was re-assigned, and a new set of auspiciousness ratings was derived using the corresponding mnemonic formula (口诀). For example, rotating a 坎宅 (sitting Zi) clockwise by 30° would result in an 艮宅 (sitting Chou), requiring the use of the 艮宅口诀 ("艮六绝祸生延天五") to assign directional stars anew.

This dynamic re-mapping is essential to preserve the internal logic of the Eight Mansions system. The method thus simulates a traditional practitioner's judgement process, translated into a computable symbolic-to-numeric interface.

Digital modelling and meteorological boundary conditions

The study site is Zhang's Mansion of the Imperial Official, located in Wanan Village, Luojiang District, Quanzhou, Fujian Province. This well-preserved Minnan-style ancestral hall features a two-courtyard axisymmetric layout with skywells (Fig. 3). The compound includes a front forecourt, main hall, intermediate court, and rear hall, with boundary walls enclosing all sides.

High-fidelity geometry was captured using oblique photogrammetry via DJI Terra and supplemented with Trimble SX10 terrestrial laser scanning. These datasets were aligned to create a detailed point cloud model. The thermally relevant geometry (walls, roofs, eaves, doors, open courts) was reconstructed in Rhino 7. Non-thermal elements (curved eaves, surface decorations) were excluded for simplification.

A computational domain extending five times the building height in all directions was constructed. Ground roughness was set to 0.03, representing rural village surfaces[8]. A uniform structured mesh was generated with a 0.5 m base cell size and boundary-layer refinement to $y^+ \approx 30$. Grid convergence was verified using the Grid Convergence Index (GCI), ensuring <5% deviation in wind speed at control points.

To simulate realistic extreme summer conditions in southern Fujian, meteorological boundary data were sourced from the Chongwu EPW file, representative of the regional climate. The hottest week (22–28 July) was selected, with average dry-bulb temperatures ranging from 25 to 36 °C and relative humidity between 67 and 83%. During this period, a dominant ESE sea breeze prevailed at ~6.76 m/s from 68°, providing a natural convective driver. These conditions align with field observations and ensure the simulation reflects a thermally critical period for human heat exposure.

To test orientation effects, the building model was rotated about its vertical axis in 15° steps, covering all 24 compass orientations. Boundary conditions (solar angles, wind direction) remained fixed in each run, and the model orientation was changed, equivalent to rotating the building in situ.

An overview of the methodological framework and simulation workflow—from data acquisition and model reconstruction to meshing, boundary conditions, and rotation across 24 orientations—is provided in Fig. 4.

Numerical simulation and thermal-comfort assessment

CFD simulations were conducted using Eddy3D v0.4.2.1 (plugin for Rhino/Grasshopper), powered by OpenFOAM 8 through blueCFD-Core 2020. The solver employed a steady-state Reynolds-Averaged Navier–Stokes (RANS) formulation with standard k–ε turbulence closure [35,36].

Boundary conditions were specified as follows: the inlet used a velocity profile matching 6.76 m/s at 10 m; the outlet used a zero-gradient condition; solid surfaces were treated as no-slip walls with a logarithmic wall function; and the sky was modelled as a symmetry plane with solar radiation mapping.

Radiative inputs were generated using Ladybug Tools, with solar position calculated from the EPW file. Mean radiant temperature (MRT) was computed using the Radiation Analysis module with 150 sun rays per

Table 1 | Feng Shui auspiciousness classification for the 24-mountain orientations (Eight Mansions)

24-mountain	Trigram (Bagua)	Star (auspicious/inauspicious)	Grade	Assigned value	Azimuth range (°)	Central azimuth (°)
Ren (壬)	Kan (坎)	Fuwei (伏位)	Slightly auspicious (小吉)	1	337.6–352.5	345
Zi (子)					352.6–7.5	0
Gui (癸)					7.6–22.5	15
Chou (丑)	Gen (艮)	Wugui (五鬼)	Quite inauspicious (次凶)	−3	22.6–37.5	30
Gen (艮)					37.6–52.5	45
Yin (寅)					52.6–67.5	60
Jia (甲)	Zhen (震)	Tianyi (天医)	Moderately auspicious (中吉)	2	67.6–82.5	75
Mao (卯)					82.6–97.5	90
Yi (乙)					97.6–112.5	105
Chen (辰)	Xun (巽)	Shengqi (生气)	Very auspicious (大吉)	4	112.6–127.5	120
Xun (巽)					127.6–142.5	135
Si (巳)					142.6–157.5	150
Bing (丙)	Li (离)	Yannian (延年)	Quite auspicious (次吉)	3	157.6–172.5	165
Wu (午)					172.6–187.5	180
Ding (丁)					187.6–202.5	195
Wei (未)	Kun (坤)	Jueming (绝命)	Very inauspicious (大凶)	−4	202.6–217.5	210
Kun (坤)					217.6–232.5	225
Shen (申)					232.6–247.5	240
Geng (庚)	Dui (兑)	Huohai (祸害)	Slightly inauspicious (小凶)	−1	247.6–262.5	255
You (酉)					262.6–277.5	270
Xin (辛)					277.6–292.5	285
Xu (戌)	Qian (乾)	Liusha (六煞)	Moderately inauspicious (中凶)	−2	292.6–307.5	300
Qian (乾)					307.6–322.5	315
Hai (亥)					322.6–337.5	330

Note: Scores range from +4 (most auspicious) to −4 (most inauspicious). Azimuth is defined with 0° at north (Zi) and increases clockwise.

hour; surface shortwave reflectances were set to 0.35 for walls, 0.20 for ground, and 0.30 for roofs.

Thermal comfort was evaluated using the Universal Thermal Climate Index (UTCI), which integrates air temperature (T_a), wind speed (v), relative humidity (RH), and mean radiant temperature (MRT) to represent human heat stress[37–39]. UTCI values at each sampling point were obtained via the Ladybug "Outdoor Comfort Calculator" component in Ladybug Tools [40].

A total of 362 sampling points were arranged within the courtyard at a height of 1.5 m above ground level, spaced approximately 0.5 m apart. For each orientation θ, the median UTCI is defined by Eq. (1):

$$UTCI_{50}(\theta) = \mathrm{Median}_{i=1}^{n}\left(UTCI_i(\theta)\right) \tag{1}$$

The orientation-wise departure from the average value is given by Eq. (2):

$$\Delta UTCI(\theta) = UTCI_{50}(\theta) - \overline{UTCI_{50}} \tag{2}$$

Analogous deviation metrics for wind speed and mean radiant temperature are shown in Eqs. (3) and (4):

$$\Delta WS(\theta) = WS(\theta) - \overline{WS} \tag{3}$$

$$\Delta MRT(\theta) = MRT(\theta) - \overline{MRT} \tag{4}$$

These were plotted as polar charts to visualise rotational symmetry and directional effects (see Fig. 6a–d).

Finally, to verify the relationship between thermal comfort and auspiciousness, two statistical tests were performed. Spearman's rank correlation coefficient ρ was calculated as defined in Eq. (5):

$$\rho = 1 - \frac{6\sum_{i=1}^{n} d_i^2}{n(n^2-1)} \tag{5}$$

Where d_i =rank (x_i) - rank(y_i), with x_i being the Feng Shui score and y_i the median UTCI for orientation i, and ($n = 24$).

Additionally, a Kruskal–Wallis H test was used to compare UTCI medians across three groups (Good: score > 0; Neutral: score = 0; Bad: score < 0), defined by Eq. (6):

$$H = \frac{12}{N(N+1)}\sum_{i=1}^{k}\frac{R_i^2}{n_i} - 3(N+1) \tag{6}$$

Where N is the total number of observations, n_i the sample size of group i, and R_i the sum of ranks in group i.

A simple OLS slope was also computed (non-inferential) to visualise the trend of UTCI across score levels. Significance was assessed at $\alpha = 0.05$.

Results

Distributional characteristics of courtyard thermal environments by orientation

The orientation of the building significantly modulates the thermal environment within the courtyard, as evidenced by the variation in median $UTCI_{50}$ across the 24 simulated orientations. Fig. 6a demonstrates a clear sinusoidal pattern in $UTCI_{50}$ distribution, with a maximum deviation of approximately 0.65 °C between the most and least favourable orientations. The most thermally comfortable alignments occurred in the range of

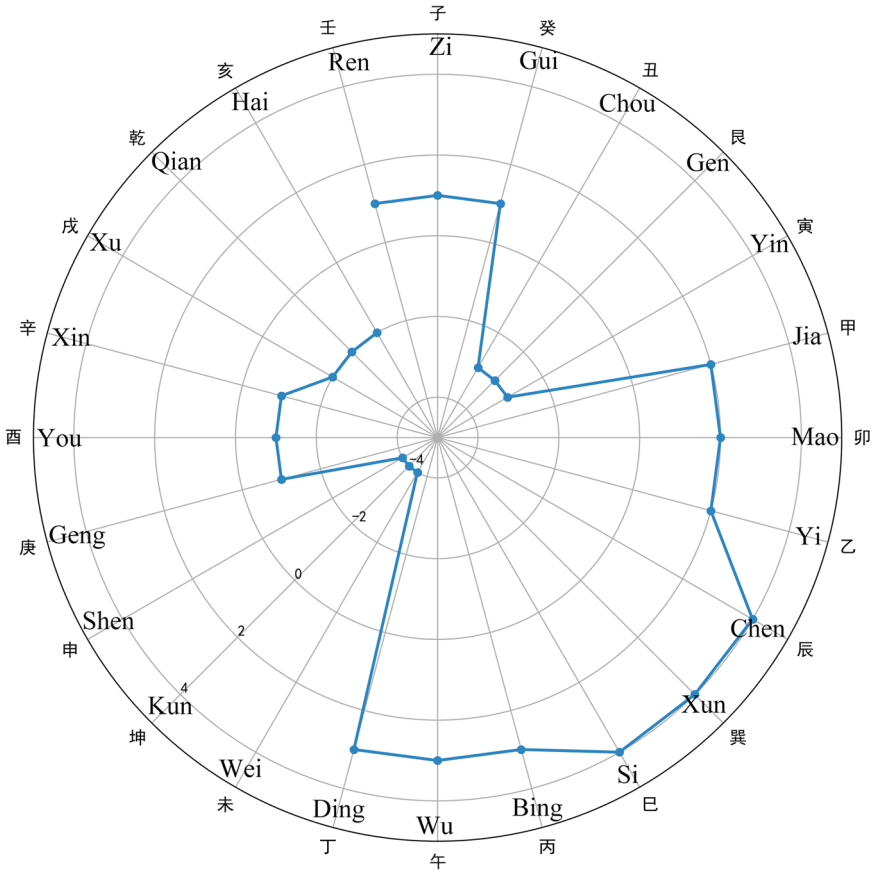

Fig. 2 | Polar plot of auspiciousness scores for the 24-mountain orientations (Eight Mansions). Outer labels show Chinese names. Scores range from −4 (most inauspicious) to +4 (most auspicious), with 0 denoting neutral. Azimuth is defined with 0° at north (Zi) and increases clockwise.

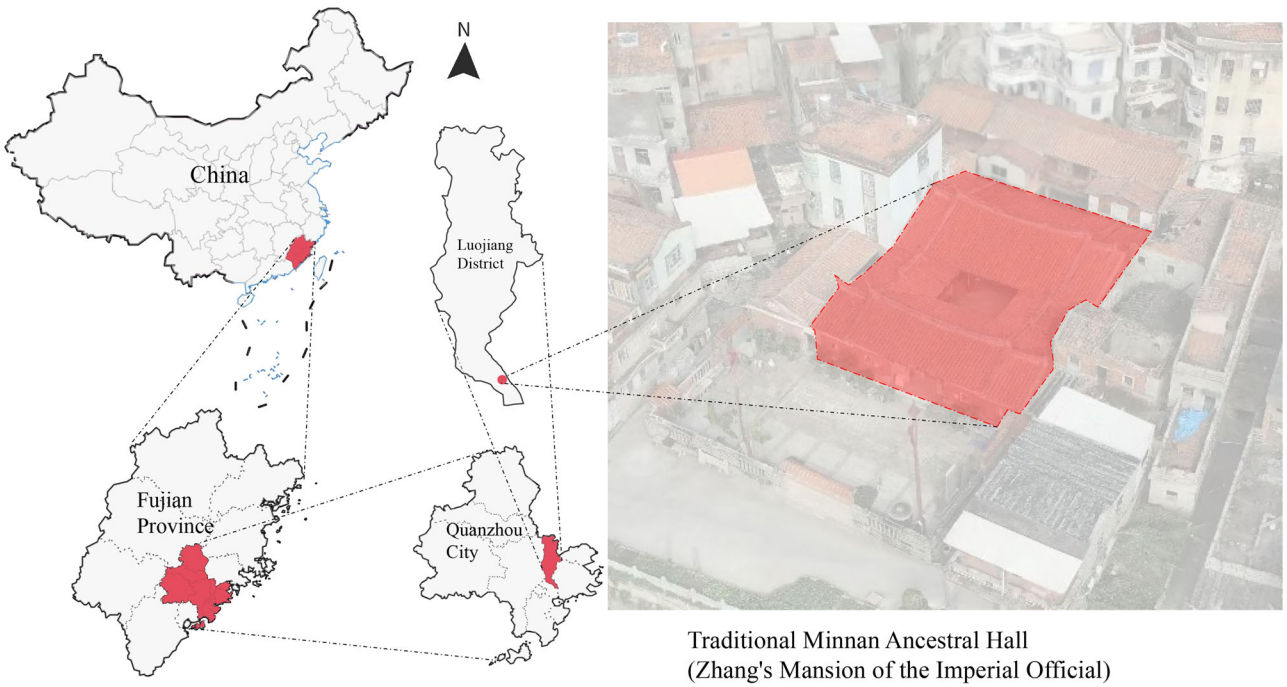

Fig. 3 | Study area and case-study site: Zhang's Mansion of the Imperial Official (Quanzhou, Fujian, China). Left: national–provincial–municipal location maps; right: orthomosaic with the case-study building highlighted. Basemap and administrative boundaries are authors' own compilations; scale bar and north arrow are shown.

105°–150° azimuth (facing ESE to SSE), which corresponds closely with the direction of the prevailing summer sea breeze (68°). This alignment effectively facilitates cross-ventilation, allowing incoming wind to sweep through the courtyard and dissipate accumulated heat.

Figure 5.Spatial distribution of UTCI under different orientations examples at 0°, 90°, and 180°).

The deviation in UTCI from the mean (ΔUTCI (θ)) reaches a minimum of −0.34 °C at 135° and a maximum of +0.31 °C at 270° as illustrated

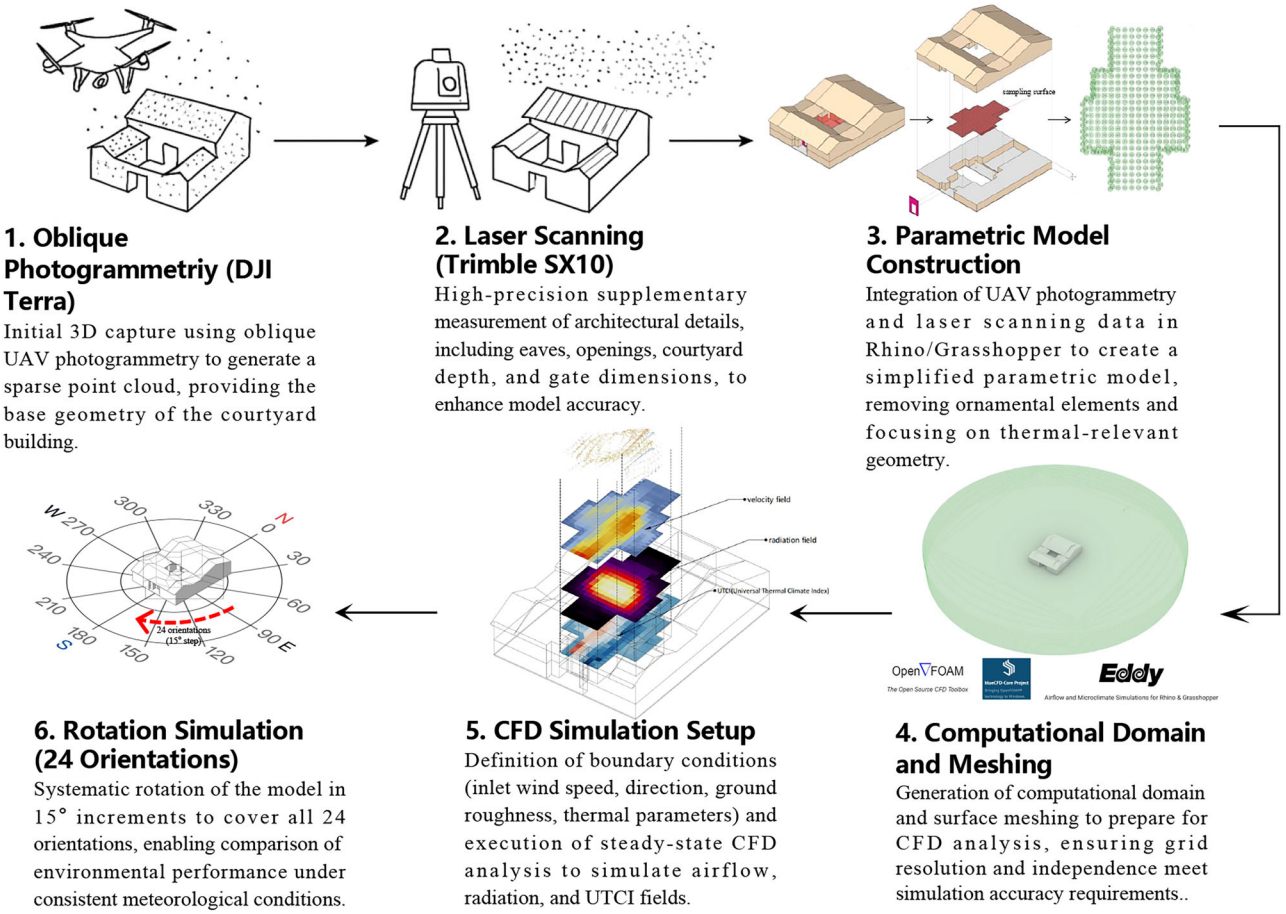

Fig. 4 | Methodological framework and simulation workflow. Steps: (1) UAV photogrammetry to capture building geometry; (2) terrestrial laser scanning for architectural details; (3) parametric simplification in Rhino/Grasshopper; (4) computational domain and meshing; (5) coupled CFD–radiation setup to compute wind speed, mean radiant temperature (MRT) and UTCI; (6) rotation experiments of the model in 15° increments to cover all 24 orientations under identical boundary conditions.

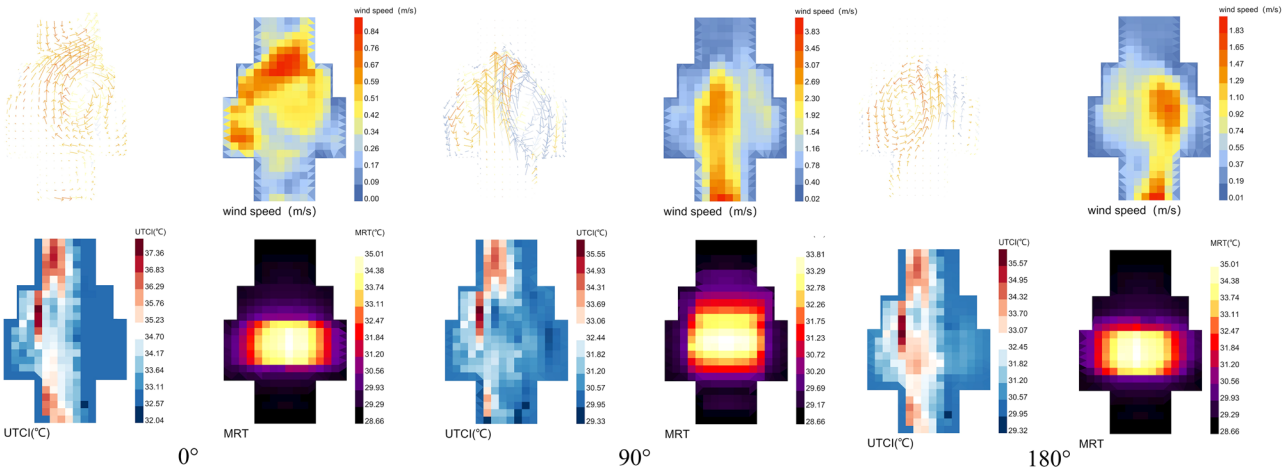

Fig. 5 | Spatial distributions for three orientations. Maps of wind speed (ms^{-1}), mean radiant temperature (MRT, °C) and UTCI (°C) for 0°, 90° and 180°. Sampling height = 1.5 m; colour scales are held constant across orientations. Azimuth is defined with 0° at north and increases clockwise.

in Fig. 6b. These extremes signify the role of ventilation corridors when the building's open facade aligns favourably with dominant wind directions. Orientations facing west (e.g., 255°–285°) typically obstruct wind inflow and trap solar heat, resulting in pronounced thermal discomfort.

While mean radiant temperature (MRT) is often the dominant contributor to thermal load, its sensitivity to orientation in this configuration appears limited. Across the orientation spectrum, ($\Delta MRT(\theta)$) fluctuates within a narrow band (±0.05 °C), indicating that changes in solar exposure due to building rotation are minor (Fig. 6d). This stability is likely due to the consistent courtyard enclosure and symmetrical massing of the ancestral hall.

By contrast, wind speed exhibits substantial orientation-dependent variability. Figure 6c shows that ($\Delta WS(\theta)$) ranges up to

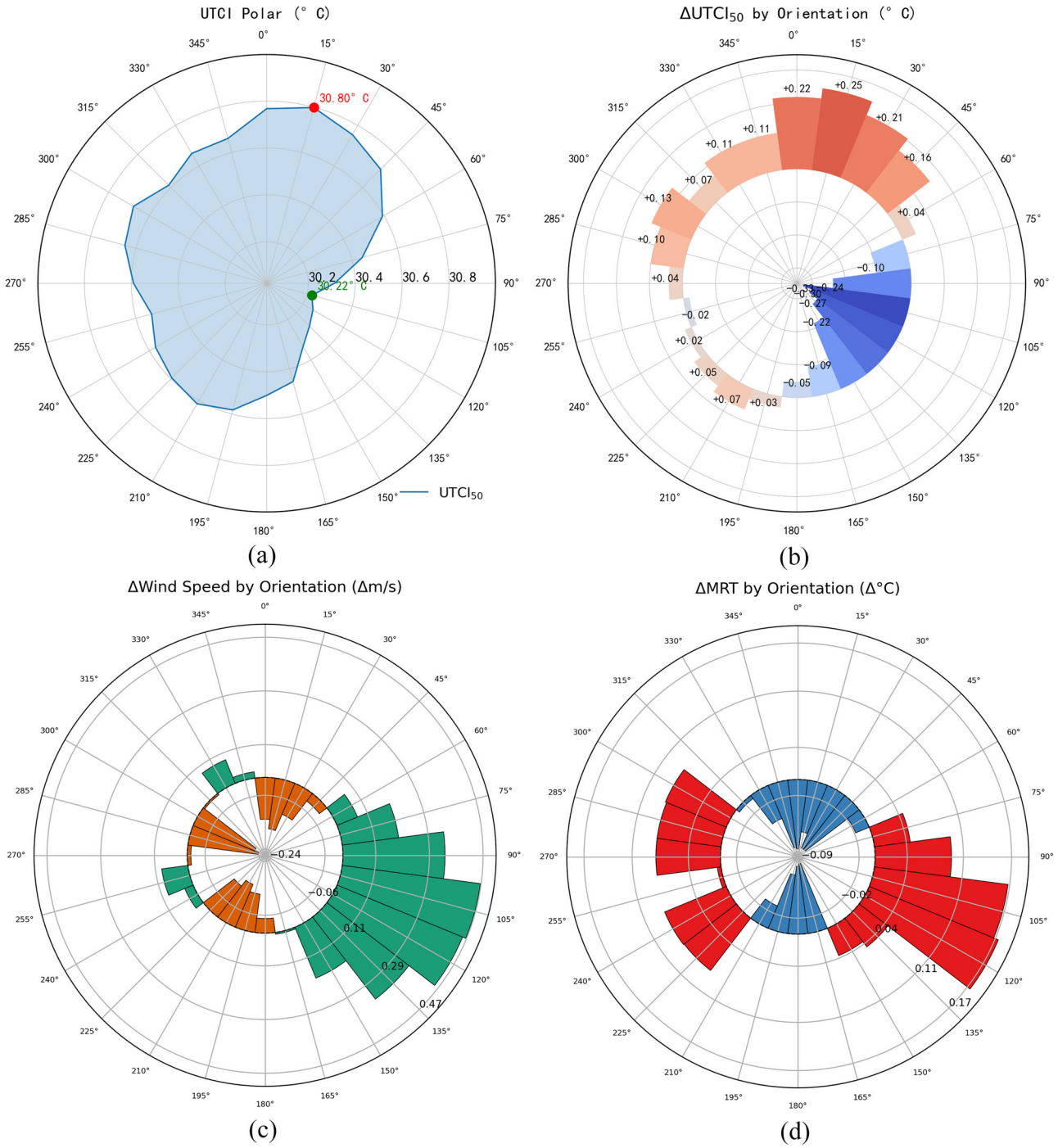

Fig. 6 | Polar summaries by orientation (15° bins). a Median UTCI ($UTCI_{50}$) across 24 orientations. **b** ΔUTCI relative to the across-orientation mean of the 24 medians (°C). **c** ΔWS relative to the across-orientation mean wind speed (ms^{-1}). **d** ΔMRT relative to the across-orientation mean MRT (°C). Shaded bands denote the interquartile range (IQR) across 362 points. Azimuth reference: 0° = north, clockwise.

±0.56 m/s, reflecting how certain orientations channel prevailing breezes into the central courtyard, while others create stagnation zones. These airflow differences are visualised in Fig. 5, where spatial maps of wind speed, MRT, and UTCI reveal ventilation corridors under favourable orientations (e.g. 90°), and recirculation under unfavourable ones (e.g., 180°).

Overall, these findings confirm that orientation plays a pivotal role in shaping the microclimate of enclosed traditional buildings—not by significantly altering radiant load, but by controlling airflow pathways and thereby modulating convective heat exchange. This highlights orientation as an actionable design parameter in climate-adaptive heritage preservation.

Figure 6. Polar plots of environmental indicators by orientation: (a) Median UTCI; (b) ΔUTCI; (c) ΔWind speed; (d) ΔMRT.

Principal drivers and mechanisms of thermal comfort in traditional courtyard dwellings

To disentangle the contributions of different environmental parameters to thermal comfort, we examined their associations with UTCI at the point level, across 362 courtyard sampling locations and 24 orientations

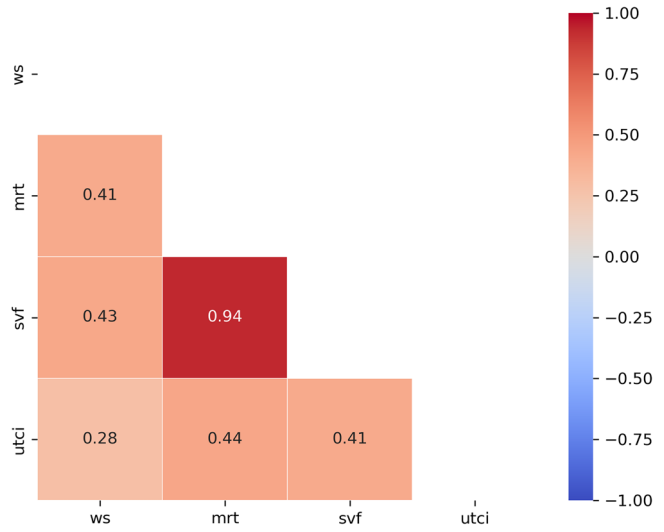

Fig. 7 | Spearman correlation matrix among UTCI, MRT, wind speed (WS) and sky view factor (SVF). Cells show correlation coefficients (ρ) with two-tailed significance; the diverging colour map is centered at 0 (range −1… +1).

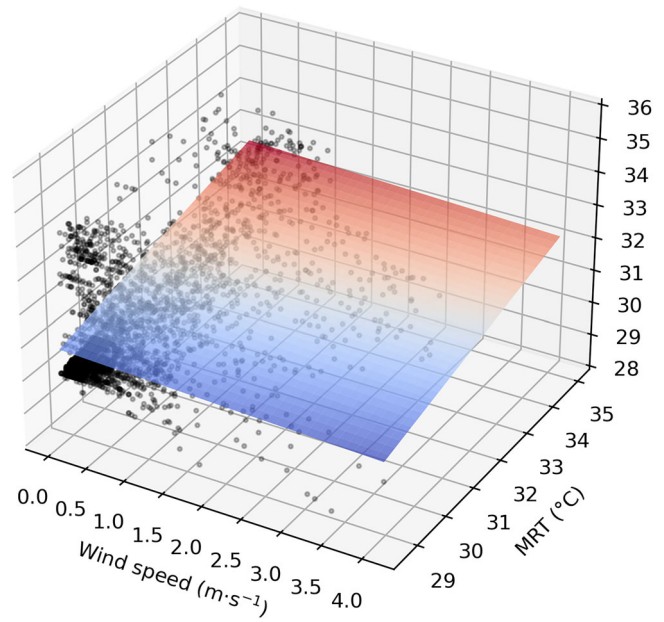

Fig. 8 | Multiple-regression surface for UTCI as a function of wind speed and MRT (ordinary least squares). The plane depicts the fitted response; grey points are individual grid cells across all orientations. Axes are WS (ms^{-1}), MRT (°C), and UTCI (°C).

(totalling 8,688 observations). Spearman correlation coefficients were computed between UTCI and three candidate variables: MRT, sky view factor (SVF), and wind speed.

As summarised in Fig. 7, UTCI is most strongly correlated with MRT ($\rho = 0.44$), affirming the central role of radiation in governing human heat stress under hot, enclosed conditions. This is consistent with the physics of the UTCI model, which attributes a significant portion of thermal load to absorbed and re-radiated solar energy. SVF also displays a moderately strong positive correlation ($\rho = 0.41$), as greater openness to the sky increases direct and diffuse solar input, thereby raising both MRT and UTCI. Wind speed, in contrast, shows a negative correlation with UTCI ($\rho = -0.28$), reflecting its mitigating effect through enhanced evaporative and convective cooling.

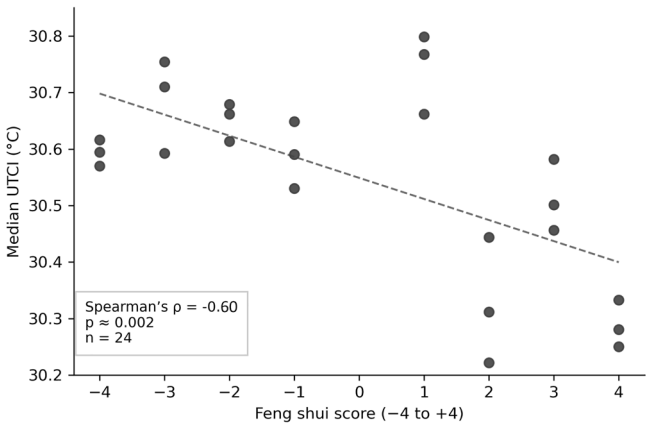

Fig. 9 | Feng Shui score vs. thermal stress. Scatter of Feng Shui auspiciousness score versus $UTCI_{50}$ across 24 orientations. Spearman's rank correlation indicates a negative association ($\rho = -0.60$, $p = 0.002$).

To further quantify these relationships, a multiple linear regression model was constructed using standardised predictors (MRT, SVF, WS). Figure 8 presents the regression results, revealing MRT as the strongest predictor (standardised coefficient = +0.28), followed by SVF (+0.14). Wind speed carries a weaker coefficient (−0.03), though its broader spatial variability, as observed in Fig. 5, suggests it may offer greater leverage in spatial design despite lower average influence.

These results indicate that although MRT dominates average UTCI values, wind speed variation is more directly modifiable through design measures such as orientation and opening placement. This distinction underscores the importance of considering both magnitude and controllability of thermal drivers in passive cooling strategies.

Explanatory power of traditional Feng Shui auspicious orientations for the thermal environment

To evaluate whether the auspicious orientations recommended by the Eight Mansions system are associated with lower thermal stress, we analysed the statistical relationship between the assigned auspiciousness scores (−4 to +4) and the simulated $UTCI_{50}$ values across all 24 orientations.

Figure 9 shows a clear inverse trend: orientations with higher auspiciousness scores tend to exhibit lower median UTCI. Spearman's rank correlation coefficient was calculated

$$\rho = -0.60^{\circ}(p = 0.002, n = 24) \quad (7)$$

This result indicates a statistically significant moderate-to-strong monotonic relationship between Feng Shui auspiciousness and thermal comfort performance.

To test whether thermal comfort differs systematically across traditional auspiciousness categories, orientations were grouped as follows: "Good" (score > 0; 9 orientations), "Neutral" (score = 0; 4 orientations), and "Bad" (score < 0; 11 orientations). A Kruskal–Wallis H test was conducted:

$$H = 15.29^{\circ}(p = 0.0005, df = 2) \quad (8)$$

The test revealed significant group-wise differences in $UTCI_{50}$. Boxplots in Fig. 10 confirm that orientations classified as 'Good' have substantially lower UTCI medians and narrower interquartile ranges compared to 'Bad' orientations. Figure 11 further illustrates this relationship using a radial plot of orientation-specific ΔUTCI grouped by auspiciousness category.

Fig. 9. Relationship between Feng Shui auspiciousness score and median UTCI.

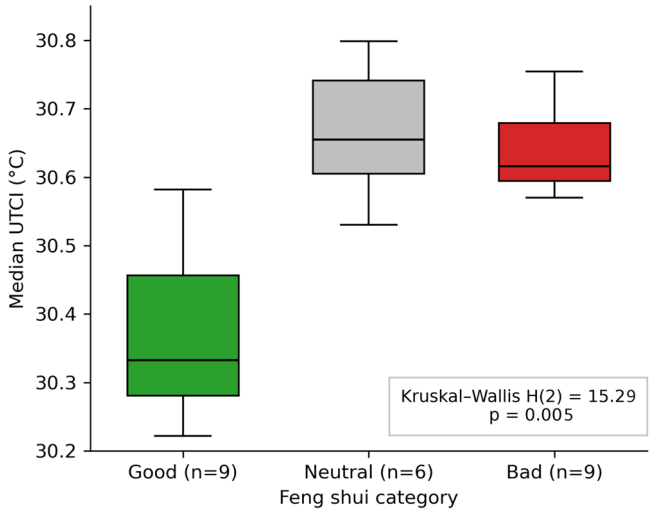

Fig. 10 | Group differences in $UTCI_{50}$ by Feng Shui category. $UTCI_{50}$ distributions for Good/Neutral/Bad categories. A Kruskal–Wallis test shows significant differences among groups (H(2) = 15.29, $p = 0.0005$). Boxes show medians and IQR; whiskers span 1.5×IQR.

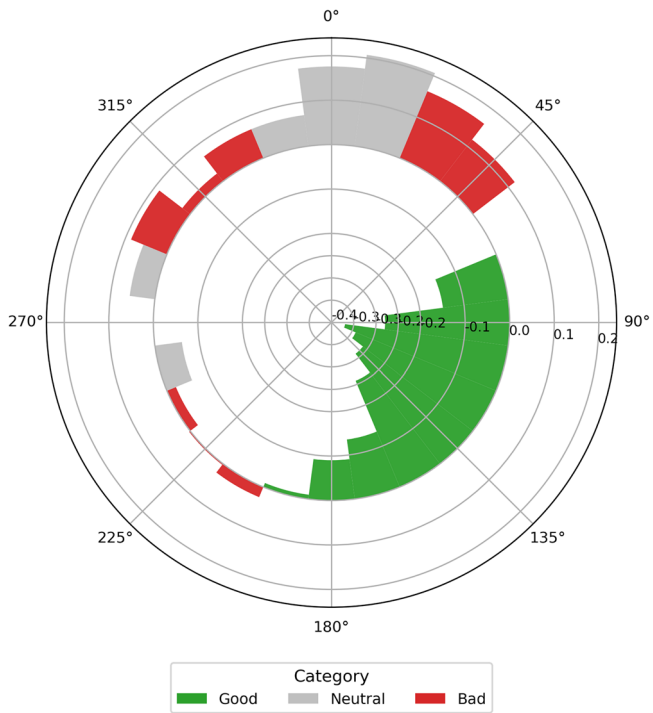

Fig. 11 | ΔUTCI by orientation (polar bars). ΔUTCI is defined as the orientation-specific median UTCI minus the across-orientation mean of the 24 medians. Observed range in this dataset: min −0.327 °C at 105°; max +0.250 °C at 15°. Axis: 0° at north, clockwise; bar width = 15°.Notes (for all Figures). UTCI Universal Thermal Climate Index, MRT mean radiant temperature, WS wind speed, SVF, sky view factor. Unless stated otherwise, 0° = north and azimuth increases clockwise; Δ indicates departure from the across-orientation mean of the same variable.

Note: Each dot is one of the 24 orientations; dashed line shows an OLS fit. Spearman's $\rho = -0.58$, permutation $p \approx 0.002$, $n = 24$. The y-axis reports median UTCI (°C).

Figure 10. UTCI by Feng Shui category (Good, Neutral, Bad).

Note: Box shows IQR with the median line; whiskers indicate 1.5×IQR. Sample sizes: Good $n = 9$, Neutral $n = 6$, Bad $n = 9$. Kruskal–Wallis H(2) = 15.28, permutation $p \approx 0.000$. colours: green = Good, gray = Neutral, red = Bad.

Figure 11 further illustrates the directional distribution of $\Delta UTCI_{50}$ grouped by Feng Shui category in 15° bins. 'Good' orientations (green), notably concentrated between 90° and 150°, show consistently negative ΔUTCI values, with the lowest median occurring at 105°. This reflects strong alignment with the prevailing summer monsoon, enabling effective convective cooling. In contrast, 'Bad' orientations (red) display scattered but elevated ΔUTCI values, with peaks near 45° and 270°, indicating misalignment with dominant wind directions and consequent thermal accumulation. The sharp clustering of green bars and the broader dispersion of red ones suggest that Feng Shui-prescribed orientations not only reduce heat stress on average, but also exhibit greater directional robustness. The polar layout visually reinforces the empirical correlation identified in the statistical tests.

Together, these findings offer quantitative evidence that the auspicious orientation logic in Eight Mansions Feng Shui aligns statistically with thermally favourable design in a hot–humid climate. This correlation bridges intangible cultural knowledge with measurable bioclimatic outcomes.

Discussion

Under the summer boundary conditions examined in this case study, orientation was associated with meaningful differences in courtyard heat stress, primarily via wind-driven convective cooling. Across the 24 rotational variants, modeled airflow aligned with the prevailing south-easterly monsoon produced lower median UTCI ($UTCI_{50}$), whereas mean radiant temperature (MRT) varied comparatively little because self-shading, eaves, and sky-view obstruction limited radiant contrast among orientations. The net inter-orientation spread in UTCI was modest in absolute magnitude (≈0.3 °C) yet systematic: orientations that faced approximately 120°–150° benefited most from cross-ventilation. In this geometry, therefore, convective removal of heat appeared to be the dominant lever, while radiation set a relatively stable background load.

These physical patterns offer a tractable way to interrogate culturally transmitted orientation heuristics. In our simulations, the best-performing orientations overlapped with categories commonly deemed "auspicious" within the Eight Mansions (Ba Zhai) system, and Feng Shui scores were negatively associated with median UTCI ($\rho = -0.60$, $p = 0.002$). We do not interpret this as proof of universal causality. Rather, we treat the correspondence as consistent with the hypothesis that orientation rules preserved in local tradition may have emerged from iterative, practice-based adaptation to seasonal winds and solar exposure, subsequently expressed through symbolic language. Framed this way, traditional prescriptions become testable, context-specific hypotheses that can be evaluated—and potentially falsified—using quantitative microclimate tools.

The Historic Urban Landscape (HUL) approach provides a useful scaffold for situating these results within a broader conservation logic. HUL emphasizes the layered integration of natural conditions, built form, and living traditions, and recognizes that intangible practices can shape spatial configuration and environmental performance. Read through this lens, our findings suggest an operational pathway that respects cultural significance while addressing climate risk: safeguard original siting and aperture alignment where feasible; maintain ventilation corridors at the building, block, and settlement scales; and screen interventions with airflow–comfort metrics (e.g., CFD coupled with UTCI). At the same time, a HUL-consistent strategy acknowledges trade-offs: ritual orientation, topography, vegetation, and surrounding massing can reinforce or counteract airflow benefits. Prescriptions should therefore be validated across seasons and typologies, complemented by community knowledge and field measurements, and adjusted to local priorities [41].

Methodologically, the study underscores two points for heritage microclimate assessment. First, models or rules of thumb that prioritize solar geometry alone may understate orientation effects in courtyard morphologies where internal airflow regimes dominate heat removal.

Explicit representation of convective processes—whether via CFD or reduced-order airflow models—can materially change comfort rankings among orientations. Second, coupling flow simulations to human-centric thermal indices provides a transparent bridge from physical fields to occupant-relevant outcomes, enabling like-for-like comparison across rotational scenarios without confounding envelope changes.

Several limitations bound the scope of inference. The analysis focuses on a single dwelling type and a peak-summer time window; performance in transitional or winter conditions was not assessed. Boundary conditions and roughness parameterizations introduce uncertainty, and the use of steady RANS cannot capture transient gusts or occupant-driven variability. Vegetation, evapotranspiration, moisture sources, anthropogenic heat, and the detailed morphologies of surrounding buildings were simplified or excluded; these factors can modulate both wind fields and MRT and warrant sensitivity tests. Culturally, our mapping of Eight Mansions categories to orientation bins was analytic and partial; the broader corpus of Feng Shui practice includes variables (e.g., site context, hydrology, ritual constraints) beyond the present scope.

Within these bounds, the study contributes three elements. First, it shows that orientation can measurably influence courtyard comfort in hot–humid settings chiefly through convective mechanisms, even when radiant loads remain relatively stable. Second, it demonstrates a pragmatic way to translate intangible heritage into falsifiable, performance-based hypotheses, creating a constructive dialogue between cultural knowledge and quantitative analysis. Third, it sketches a HUL-aligned, operations-level pathway—retain or recover beneficial alignments, preserve ventilation corridors, and evaluate changes with airflow–comfort metrics—that links conservation practice to climate-adaptation goals.

Future research should extend the temporal and typological scope (multi-season, multi-year, and multi-building settlements), incorporate explicit modeling of vegetation and surrounding mass, and integrate in-situ measurements for joint validation of airflow, radiation, and comfort metrics. Comparative studies across climatic regions could test whether the observed correspondence between traditional orientation rules and comfort holds beyond this context or fragments along local wind regimes. Within its stated limits, the present case study illustrates that culturally embedded orientation practices can be interrogated with modern microclimate tools and, under certain conditions, may align with physical mechanisms that mitigate thermal stress.

Data availability

The minimal dataset underlying this study—including the simplified geometry, boundary-condition notes for the hottest week, the 24-mountain (Ba Zhai) orientation mapping, point-level results for 362 sampling points across 24 orientations, aggregated statistics (Spearman, Kruskal–Wallis, correlation matrices), and vector figures—is archived at Zenodo (DOI: 10.5281/zenodo.17355160). The repository also provides documentation of software versions and reproduction steps. Meteorological boundary data were obtained from the Chongwu EnergyPlus EPW and are referenced via URL in the repository; the EPW file itself is not redistributed due to third-party licensing. For peer review, editors and reviewers have been given a private access link; the record will be publicly accessible upon publication.Code availabilityAll custom code used for preprocessing, CFD post-processing, UTCI computation and figure generation—together with the Grasshopper definition used to set up the 24 orientation scenarios—is archived in the same Zenodo record (DOI: 10.5281/zenodo.17355160) under the /code directory. The repository includes an environment.yml and a plugins_versions.txt detailing Rhino/Grasshopper, Ladybug Tools, Eddy3D and OpenFOAM versions to facilitate reproducibility. Source code is released under the MIT License; dataset files are released under CC BY 4.0 as noted in the record.

Code availability

All custom code used for preprocessing, CFD post-processing, UTCI computation and figure generation—together with the Grasshopper definition used to set up the 24 orientation scenarios—is archived in the same Zenodo record (DOI: 10.5281/zenodo.17355160) under the /code directory. The repository includes an environment.yml and a plugins_versions.txt detailing Rhino/Grasshopper, Ladybug Tools, Eddy3D and OpenFOAM versions to facilitate reproducibility. Source code is released under the MIT License; dataset files are released under CC BY 4.0 as noted in the record.

Received: 21 October 2025; Accepted: 26 December 2025;
Published online: 10 January 2026

References

1. IPCC. *Climate Change 2023: Synthesis Report* (Intergovernmental Panel on Climate Change, 2023).
2. United Nations Environment Programme (UNEP). *2023 Global Status Report For Buildings and Construction: Towards a Zero-emissions, Efficient and Resilient Buildings and Construction Sector* (GlobalABC/UNEP, 2023).
3. Santamouris, M. On the energy impact of urban heat islands and global warming on building energy consumption. *Energy Build.* **82**, 100–113 (2014).
4. Elaouzy, Y. & El Fadar, A. Energy, economic and environmental benefits of integrating passive design strategies into buildings: a review. *Renew. Sustain. Energy Rev.* **167**, 112828 (2022).
5. Li, J. The bioclimatic features of vernacular architecture in China. *Renew. Energy* **8**, 305–308 (1996).
6. Zhang, F. et al. Climate adaptability based on indoor physical environment of traditional dwelling in North Dong areas, China. *Sustainability* **14**, 850 (2022).
7. Wang, Y., Li, X. & Gan, Y. Study on the green design strategies of "neo-vernacular architecture. *Procedia Eng.* **169**, 367–374 (2016).
8. Sun, Y. Passive house: a practice of low carbon and sustainable development in China. *Appl. Comput. Eng.* **3**, 122–127 (2023).
9. Wang, Q.-H. *Fengshui Lilun Yanjiu [Research on Feng Shui theory]* (Tianjin Univ. Press, 2005).
10. Cheng, J.-J. *Feng Shui yu Jianzhu [Feng Shui and architecture]* (Central Compilation & Translation Press, 2010).
11. Liang, X. Cong jiluo xuanzhi kan Zhongguoren de fengshui guan [The Chinese concept of Feng Shui viewed from settlement site selection]. *New Architecture* **4**, 67–71 (1988).
12. Liu, P.-L. Fengshui moshi de dilixue pingjia [A geographical evaluation of the Feng Shui model]. *Human Geogr.* **1**, 36–39 (1996).
13. Mak, M. Y. & Ng, S. T. The art and science of Feng Shui—a study on architects' perception. *Build. Environ.* **40**, 427–434 (2005).
14. Li, B., Guo, W., Schnabel, M. A. & Moleta, T. Feng-Shui and computational fluid dynamics: analysing natural ventilation and human comfort. *J. Asian Archit. Build. Eng.* **19**, 329–340 (2020).
15. Bruun, O. *Fengshui in China: Geomantic Divination between State Orthodoxy and Popular Religion* (NIAS Press, 2003).
16. Luo, Y. Kejia minjian fengshui xinyang yanjiu—yi Gannan wei zhongdian de kaocha [A study of Hakka folk Feng Shui beliefs—A focused investigation in southern Jiangxi]. *J. Guangxi Univ. Natl. (Philos. Soc. Sci. Ed)* **32**(3), 2–9 (2010).
17. Cheng, A.-Q. Lun "fengshui xueshuo" dui Kejia tulou de yingxiang [The influence of "Feng Shui theory" on Hakka earth buildings]. *J. Guangxi Univ. Natl. (Philos. Soc. Sci. Ed)* **3**, 76–82 (2002).
18. Han, K.-T. Empirical and quantitative studies of Feng Shui: a systematic review (PRISMA 2009 item 1). *Heliyon* **9**, e19532 (2023).
19. Matthews, M. R. *Feng Shui: Teaching about Science and Pseudoscience* https://doi.org/10.1007/978-3-030-18822-1 (Springer, 2019).
20. Shokri, A., Shieh, E. & Vahid, A. Urban Feng Shui based on citizenship rights and its impact on the spatial structure and mental health of citizens. *Ann. Med. Surg.* **85**, 104921 (2023).
21. Zhang, S. The heritage practices in a Chinese historic neighbourhood: the manifestation of traditional Feng Shui in Langzhong, China. *Int. J. Herit. Stud.* **24**, 531–546 (2018).

22. Bo, S. Traditional Feng Shui Architecture as an Inspiration for the Development of Green Buildings. *eJournal of Public Affairs* **3**, 5 https://doi.org/10.21768/ejopa.v3i2.5 (2014).
23. Guo P, Ding C, Guo Z, et al. Coupling CFD simulation and field experiments in summer to prove Feng Shui optimizes courtyard wind environments: a case study of Prince Kung's Mansion in Beijing. *Buildings*. **12**, 629 https://doi.org/10.3390/buildings12050629 (2022).
24. Zhao, Z., Zhang, S. & Peng, Y. Analysis of winter environment based on CFD simulation: a case study of Long-Hu Sand Feng Shui layout at Jiangxi Bailudong Academy Complex. *Buildings* **13**, 351 (2023).
25. Zhou, Z. et al. Physical environment study of traditional village patterns in Jinxi County, Jiangxi Province based on CFD simulation. *Processes* **10**, 1549 (2022).
26. Wang, Z., Liu, T., Wu, X., Chen, J. & Liang, X. Influence of doorway position on wind comfort in Beijing quadrangle dwellings. *Buildings* **13**, 2557 (2023).
27. Azimi, Z. & Shafaat, A. Proposing design strategies for contemporary courtyards based on thermal comfort in cold and semi-arid climate zones. *Build. Environ.* **266**, 112150 (2024).
28. Nasrollahi, N., Hatami, M., Khastar, S. R. & Taleghani, M. Numerical evaluation of thermal comfort in traditional courtyards to develop new microclimate design in a hot and dry climate. *Sustain. Cities Soc.* **35**, 449–467 (2017).
29. Du, X., Bokel, R. & van den Dobbelsteen, A. Spatial configuration, building microclimate and thermal comfort: a modern house case. *Energy Build.* **193**, 185–200 (2019).
30. Iskandar, L., Bay-Sahin, E., Martinez-Molina, A. & Toker Beeson, S. Evaluation of passive cooling through natural ventilation strategies in historic residential buildings using CFD simulations. *Energy Build.* **308**, 114005 (2024).
31. Okafor, M. U., Awuzie, B. O., Otasowie, K., Marcel-Okafor, U. & Aigbavboa, C. Evaluation of indoor thermal comfort conditions of residential traditional and modern buildings in a warm-humid climate. *Sustainability* **14**, 12138 (2022).
32. Binarti, F., Koerniawan, M. D., Triyadi, S., Utami, S. S. & Matzarakis, A. A review of outdoor thermal comfort indices and neutral ranges for hot-humid regions. *Urban Clim.* **31**, 100531 (2020).
33. Yang, Y. *Si Ku Cun Mu: Qing Li Hui Kan 10 Zeng Tu Ba Zhai Ming Jing* (Huaxia Publishing House, 2020).
34. Wang, J. *Yang zhai shi shu* (Traditional Chinese Medicine Ancient Books Publishing House, 2020).
35. Kastner, P. & Dogan, T. Eddy3D: a toolkit for decoupled outdoor thermal comfort simulations in urban areas. *Build. Environ.* **212**, 108639 (2022).
36. Tamura, T. et al. Numerical prediction of wind loading on buildings and structures: activities of AIJ cooperative project on CFD. *J. Wind Eng. Ind. Aerodyn.* 67–68 https://doi.org/10.1016/S0167-6105(97)00109-8 (1997).
37. Vatani, J., Golbabaei, F., Dehghan, S. & Yousefi, A. Applicability of Universal Thermal Climate Index (UTCI) in occupational heat stress assessment: a case study in brick industries. *Ind. Health* **54**, 14–19 (2015).
38. Nassiri, P. et al. Application of Universal Thermal Climate Index (UTCI) for assessment of occupational heat stress in open-pit mines. *Ind. Health* **55**, 437–443 (2017).
39. Thapa, S., Rijal, H. & Zaki, S. District-wise evaluation of meteorological factors and outdoor thermal comfort in India using UTCI—Insight into future climatic scenario. *Sustain. Cities Soc.* **116**, 105840 (2024).
40. Roudsari, M. S. & Pak, M. Ladybug: a parametric environmental plugin for Grasshopper to help designers create an environmentally-conscious design. In *Proc. Building Simulation 2013: 13th International Conference of the International Building Performance Simulation Association (BS2013)* (ed. Wurtz, E.) 3128–3135 (International Building Performance Simulation Association, 2013).
41. UNESCO. Recommendation on the Historic Urban Landscape (HUL), 36 C/Resolution 41. UNESCO https://whc.unesco.org/en/hul/ (2011).

Acknowledgements

This research was funded by the Hainan Provincial Natural Science Foundation of China (Grant No. 725RC790), project titled "Research on Historical Urban Landscape Space Perception and Recreational Experience in Haikou Based on Digital Technology".

Author contributions

T.F.L. conceived and supervised the study. Y.W. (Yaolong Wang) and T.F.L. designed the research framework. Y.W., J.X. and L.W. developed the methodology and software workflow (CFD/UTCI pipeline), with validation by T.F.L. and Y.N.S. Z.W. (Zefa Wang), F.T. and T.H. conducted surveying, modelling and data curation. Y.N.S. and Y.W. performed the formal analysis and visualisation. Y.N.S. and Y.W. drafted the manuscript; T.F.L. led critical revision. All authors discussed the results and approved the final manuscript.

Competing interests

The authors declare no competing interests.

Additional information

Correspondence and requests for materials should be addressed to Tingfeng Liu or Zefa Wang.